SUPPLEMENTARY INFORMATION

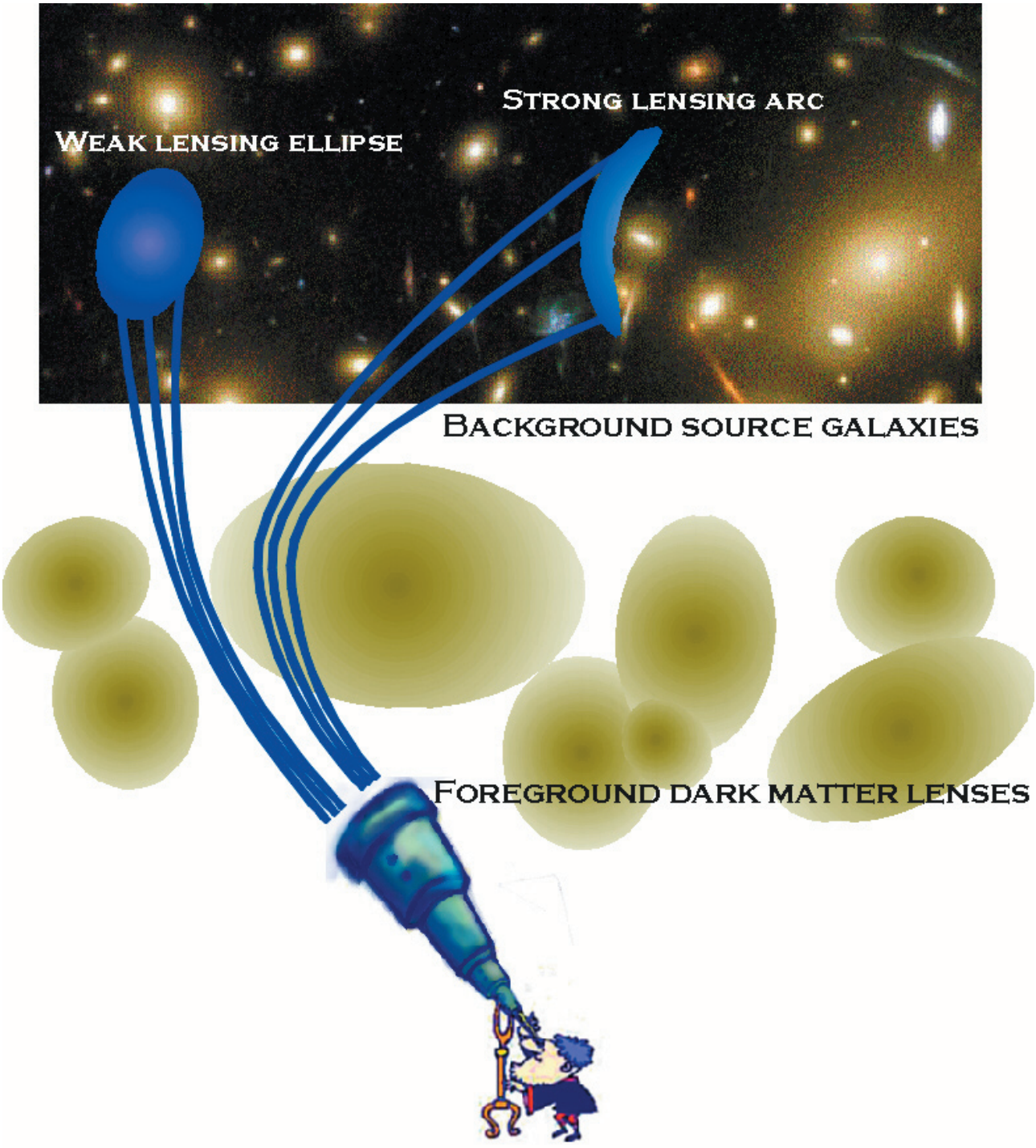

Figure S1 | Cartoon illustrating the process of gravitational lensing. Gravitational lensing by foreground mass distorts the shapes of distant galaxies, regardless of the nature of that mass. It is thus sensitive to the dominant contribution of dark matter. Measuring these distortions to infer the intervening distribution of dark matter is like studying bent lines of text through a magnifying glass to study the properties of the glass lens. Along lines of sight including the most dense mass concentrations, ***strong gravitational lensing*** distorts individual background galaxy shapes into multiply-imaged giant arcs. Along a more typical line of sight, the modest ***weak gravitational lensing*** induces a 2-3% change of ellipticity. In this regime, the lensing distortion is smaller than the typical variation between galaxy morphologies, and it cannot be measured from a single galaxy because its intrinsic shape is not observable. However, the signal can still be detected statistically. The intrinsic shapes of adjacent galaxies are unrelated so, in the absence of lensing, they should have no preferred orientation. On the other hand, when adjacent galaxies have been lensed by approximately the same intervening mass, the weak lensing signal can be recovered from the degree of correlation between their shapes.

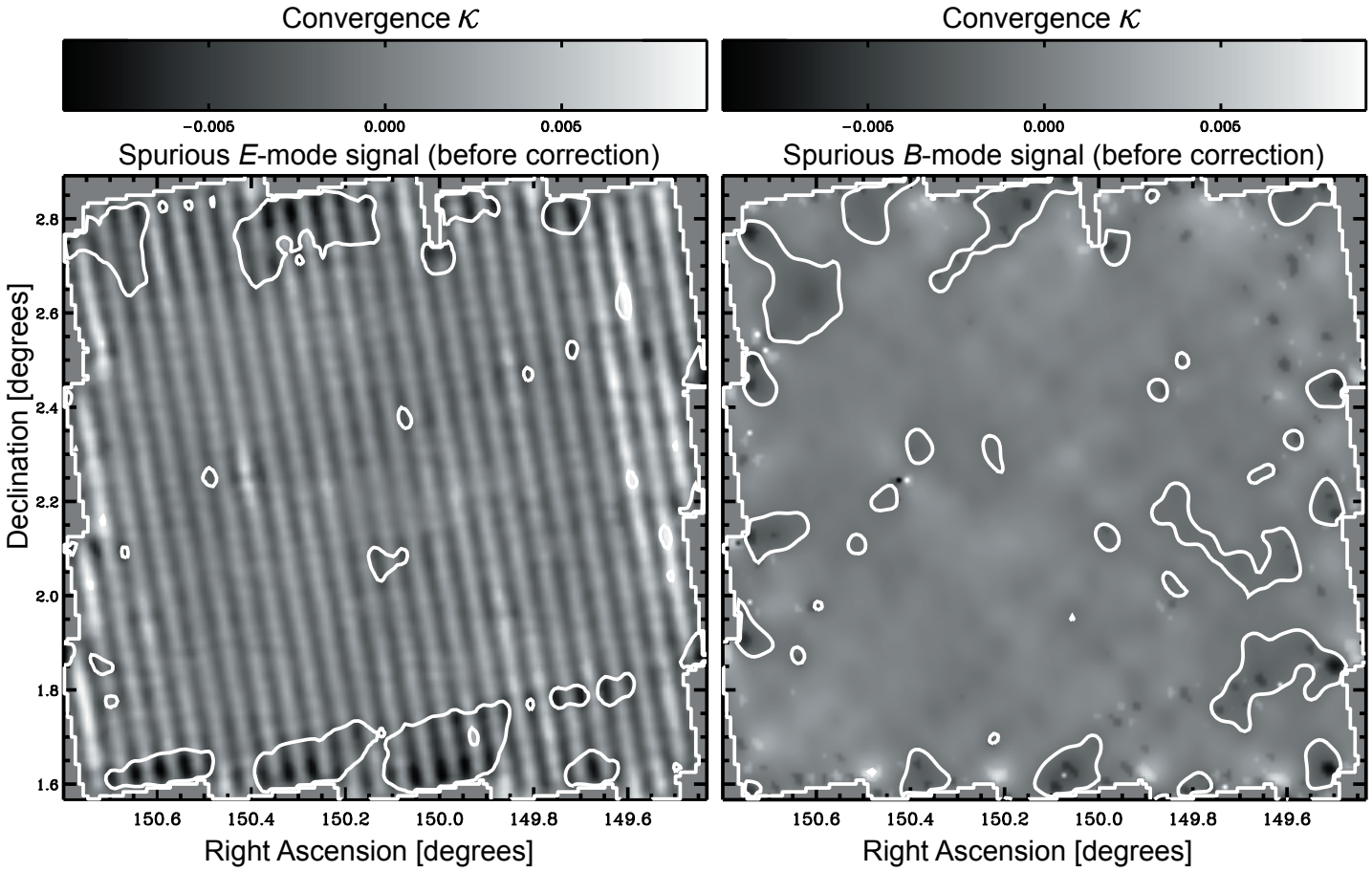

Figure S2 | Spurious signal due to imperfect Charge Transfer Efficiency (CTE) ***before correction***. The continual bombardment of spacecraft electronics by high energy particles degrades detectors' CTE. During CCD readout, defects in the silicon substrate act as charge traps that trail the image in the readout direction, mimicking a weak lensing signal. Deterioration continued during the two years of observations, and the spurious signal is worse at the edges of the field than in the middle, because of the approximately spiral pattern in which the data were obtained. CTE trailing is of particular concern in this data set because the arrangement of the *HST ACS* CCDs places spurious signal entirely into the measured *E*-mode (left panel), with no coherent *B*-mode counterpart (right panel). In this respect, it is unlike most other expected sources of observational systematics. To highlight the oscillatory, sawtooth pattern created by the CCD configuration, the greyscale image shows a reconstruction of our model of the spurious signal with twice the resolution (0.6' FWHM) to that used in the mass maps (Fig. 1 in the main article). This most clearly reveals the sawtooth pattern, but is only possible because our CTE model contains no noise. The contours, which are drawn at the same levels as those in Fig. 1, show the reconstruction after the same amount of smoothing used the real mass map. After this smoothing, the mean peak height across the reconstruction is 0.1%. The conversion of shear to convergence involves a complex iteration over scales, and this provides the most appropriate estimate of the (uncorrected) signal due to CTE effects.

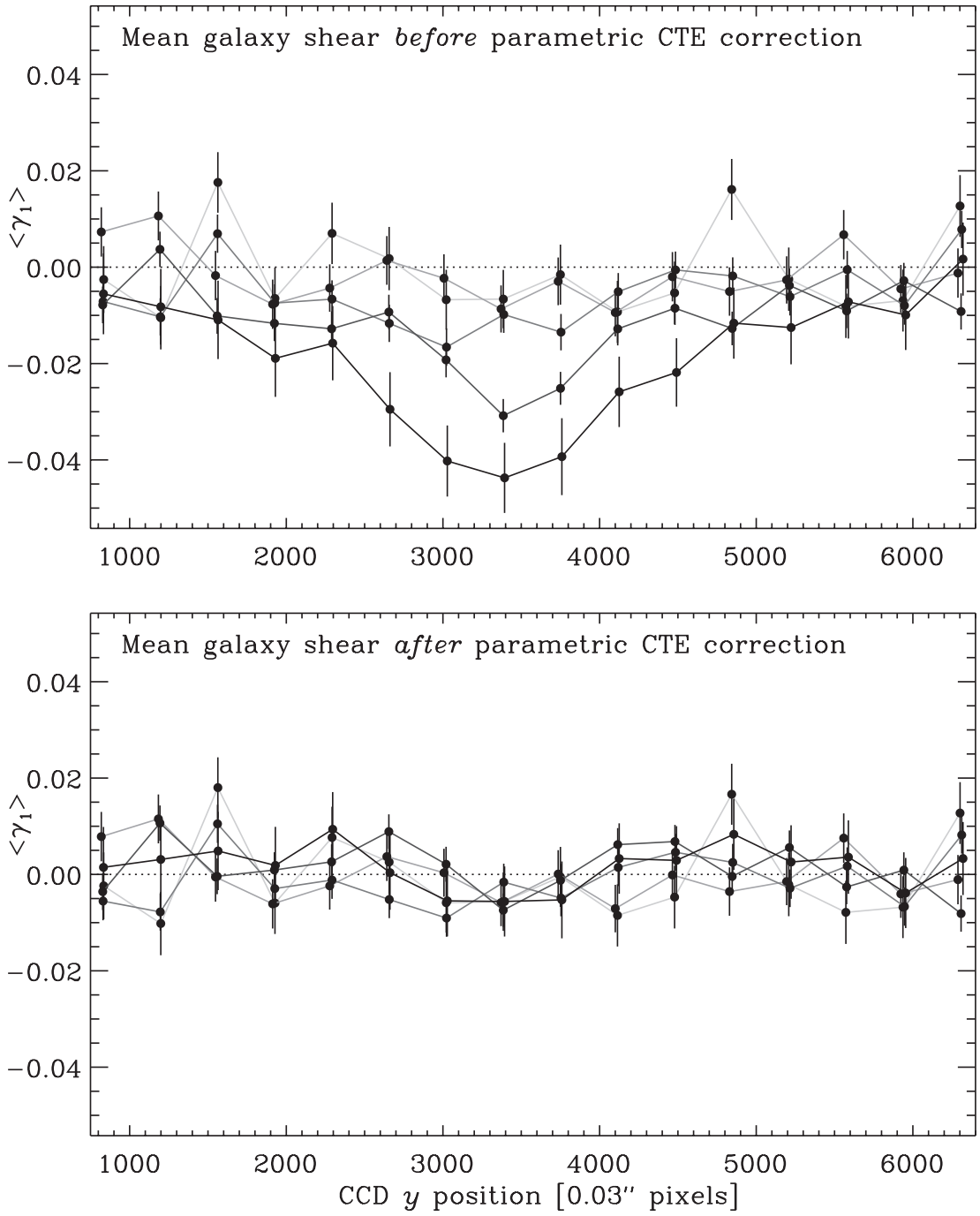

Figure S3 | Correction for Charge Transfer Efficiency (CTE). The spurious CTE signal can be measured independently by directly stacking galaxies from many different pointings as a function of their position on the CCD. Since the images cover different patches of sky, the cosmological signal averages away. The top panel shows the spurious vertical (negative) elongation of galaxies before correction. The ACS CCDs have readout registers at the top and bottom of the field of view, so the CTE signal is worst in a band across the middle. The top (light coloured) line is for bright galaxies between *F814W* magnitudes 22 and 23; the other lines are in increments of one magnitude, continuing to the faintest and most affected galaxies between magnitudes 26 and 27 in the bottom (dark coloured) line (s.e.m. errors). The bottom panel shows the residual signal after applying our parametric correction to the shear catalogue. This reduces the signal by a further factor of at least 5 (stronger statements would require an even larger survey to test). Using this model correction in the mass reconstruction takes the peak convergence level below 0.1%. Reproduced from Rhodes et al. (2007), with permission from the Astrophysical Journal.

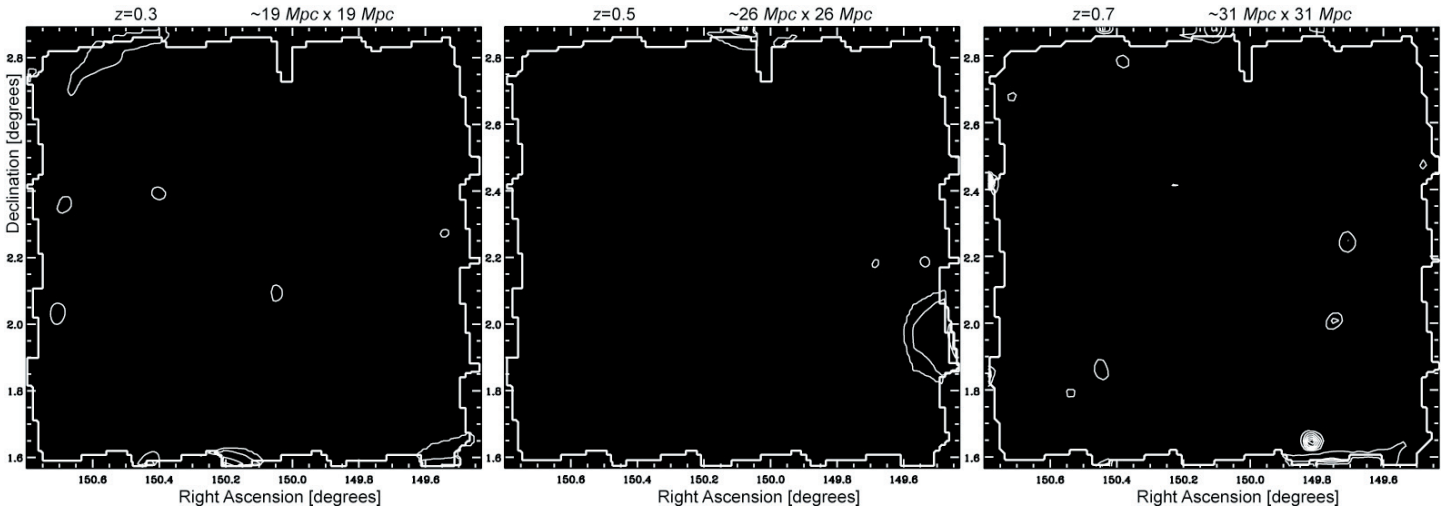

Figure S4 | Realisation of noise level in the tomographic mass reconstructions. These show the "*B*-mode" signal from galaxy populations restricted to redshift slices, and are expected to be consistent with zero in the absence of systematic effects. Contours are drawn at the same levels as those in the "*E*-mode" weak lensing maps (Fig. 4). Judging by the ratio of the pixels above and below the contours as before, and assuming Gaussian noise distribution, the second contour corresponds to ~3σ significance.

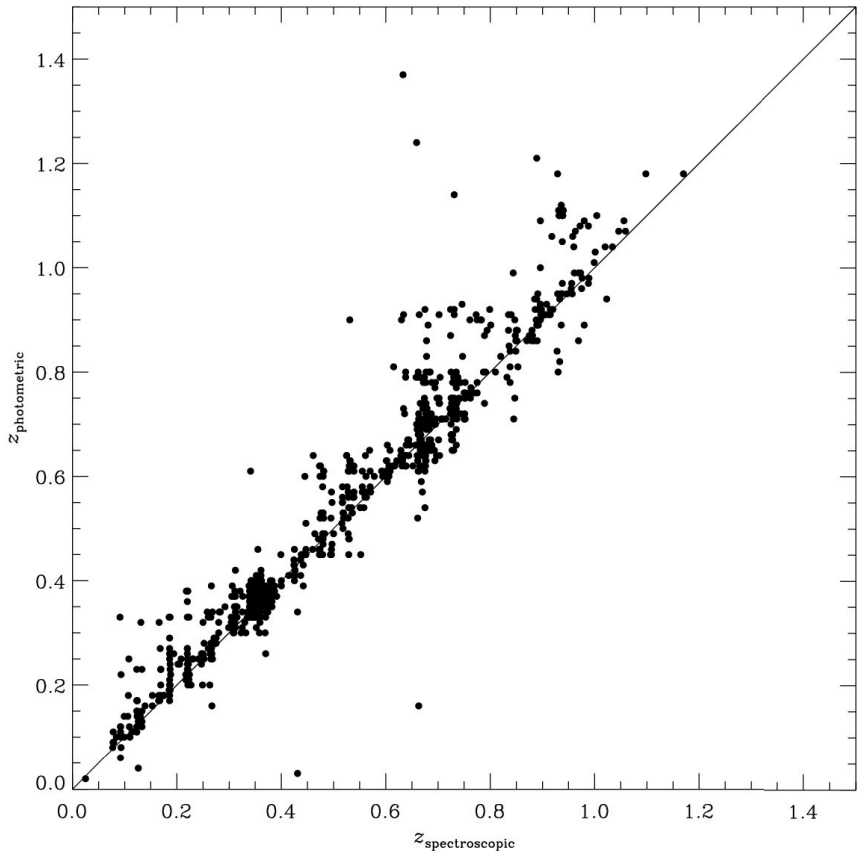

Figure S5 | Photometric redshift accuracy for bright galaxies. This demonstrates the $\delta z \approx 0.15$ performance of our photometric redshift estimation in a sample of 822 relatively bright (*F814W*>*22.5*) galaxies for which spectroscopic redshift are available. Accuracy inevitably degrades for fainter galaxies, which make up the majority of our source population. In particular, these are subject to "catastrophic" failures, which we treat asymmetrically using our novel statistical method described in the main article.

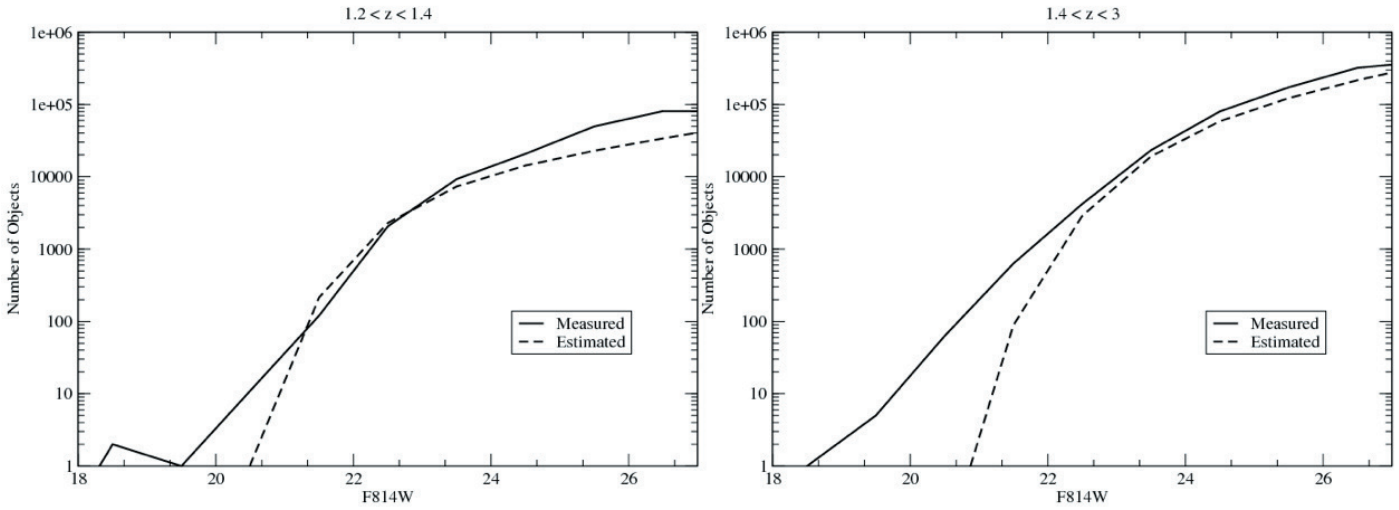

Figure S6 | Measured and expected number counts of faint galaxies. Shown as a function of apparent magnitude for galaxies in redshift bins $1.2<z<1.4$ and $1.4<z<3$. Notice the two are in good agreement except at the bright and faint ends. This disagreement is quantified in supplementary table S1.

F814W magnitude	Redshift		
	1.0→1.2	1.2→1.4	1.4→3.0
20.5	2.8	10.6	926
21.5	1.2	1	7.1
22.5	1.05	1	1.46
23.5	1	1.26	1.22
24.5	1	1.45	1.36
25.5	1.5	2.17	1.41
26.5	1.5	2.4	1.48
Total	1.19	1.74	1.39

Table S1 | Dilution of the lensing signal by the spurious inclusion of low redshift galaxies at high redshift. The numbers are the ratio of the number of galaxies observed in each redshift bin (including those with incorrect photometric redshifts) to the number expected from external measurements of the galaxy luminosity function between $z=1.2$ and $z=3$. The total shows the dilution in each redshift bin, accounting for the distribution of galaxies of various magnitudes.

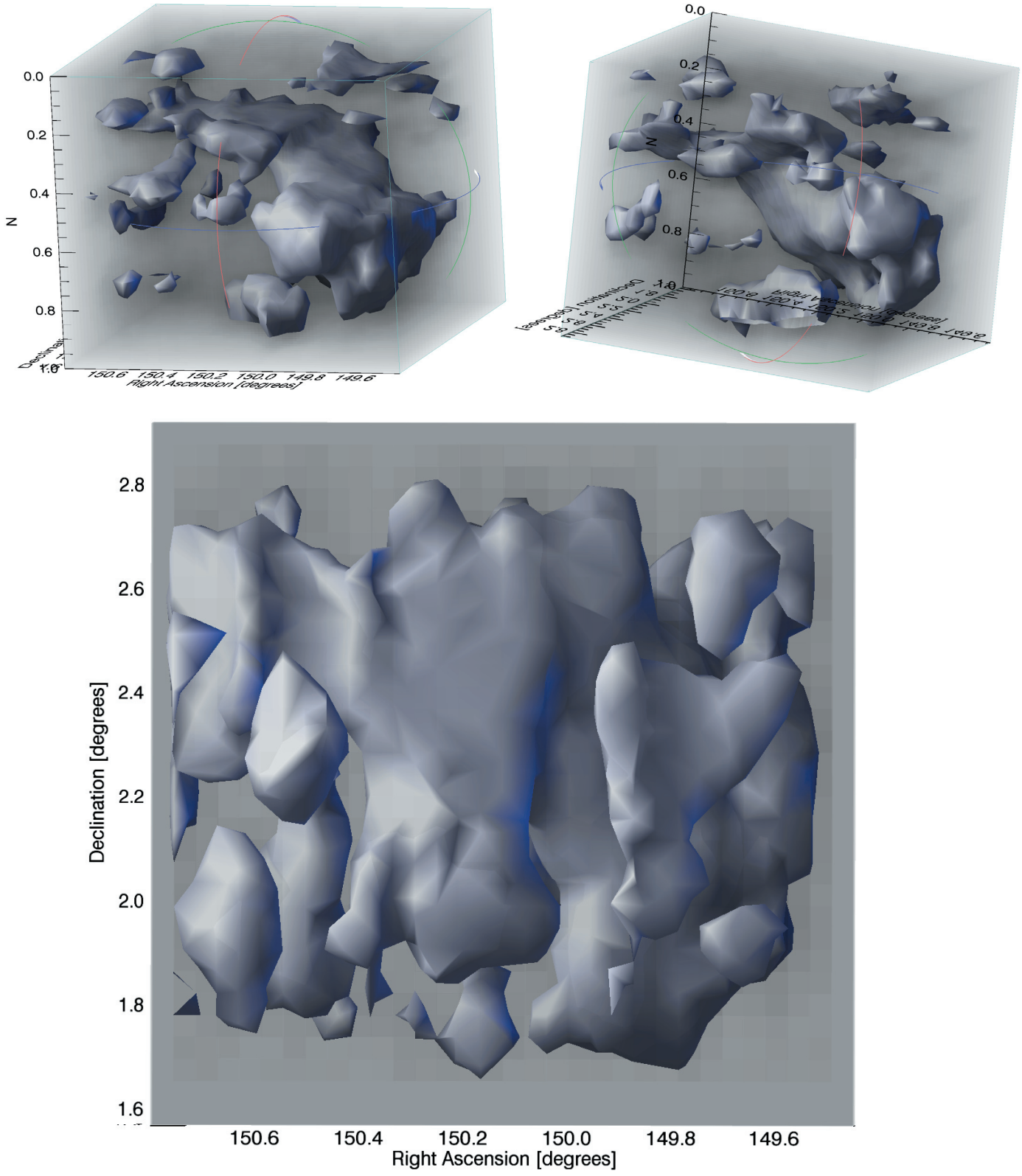

Figure S7 | Additional views of the 3D mass reconstruction. In the lower panel, it is seen from the perspective of Earth, as with the projected and tomographic mass maps in the main article.